Radical chemistry in the Pearl River Delta: observations and modeling of OH and HO₂ radicals in Shenzhen 2018

Xinping Yang[1,2], Keding Lu[1,2,*], Xuefei Ma[1,2], Yue Gao[1,2], Zhaofeng Tan[3], Haichao Wang[4], Xiaorui Chen[1,2], Xin Li[1,2], Xiaofeng Huang[5], Lingyan He[5], Mengxue Tang[5], Bo Zhu[5], Shiyi Chen[1,2], Huabin Dong[1,2], Limin Zeng[1,2], Yuanhang Zhang[1,2,*]

[1]State Key Joint Laboratory of Environmental Simulation and Pollution Control, College of Environmental Sciences and Engineering, Peking University, Beijing, China

[2]State Environmental Protection Key Laboratory of Atmospheric Ozone Pollution Control, Peking University, Beijing, China

[3]Institute of Energy and Climate Research, IEK-8: Troposphere, Forschungszentrum Juelich GmbH, Juelich, Germany

[4]School of Atmospheric Sciences, Sun Yat-Sen University, Zhuhai, China

[5]Laboratory of Atmospheric Observation Supersite, School of Environment and Energy, Peking University Shenzhen Graduate School, Shenzhen, China

Correspondence to: Keding Lu (k.lu@pku.edu.cn), Yuanhang Zhang (yhzhang@pku.edu.cn)

Abstract. The ambient ~~OH and HO₂ radical~~ concentrations were measured continuously by laser-induced fluorescence during the STORM (STudy of the Ozone foRmation Mechanism) campaign at the Shenzhen site, located in the Pearl River Delta in China, in autumn 2018. The diurnal ~~maximum~~ maxima were ~~OH and HO₂ concentrations, measured by laser-induced fluorescence, were~~ 4.5×10^6 cm⁻³ for OH and 4.5×10^8 cm⁻³ for HO₂ (including an estimated interference of 23%-28% from RO₂ radicals during the daytime), respectively. The state-of-the-art ~~radical~~ chemical mechanism underestimated the observed OH concentration, similar to the other warm-season campaigns in China. The OH underestimation was attributable to the missing OH sources, which can be explained by the X mechanism. Good agreement between the observed and modeled OH concentrations was achieved when an additional numerical X equivalent to 0.1 ppb NO concentrations was added to the base model. The isomerization mechanism of RO₂ derived from isoprene contributed approximately 7% to the missing OH sources and the oxidation of isoprene oxidation products (MACR and MVK) had no significant impact on the missing OH sources, demonstrating further exploration of unknown OH sources is necessary. ~~The modeled HO₂ could reproduce the observed HO₂, indicating the HO₂ heterogeneous uptake on HO₂ chemistry was negligible.~~ Photolysis reactions dominated the ROx primary production rate. The HONO, O₃, HCHO, and carbonyls photolysis accounted for 29%, 16%, 16%, and 11% during the daytime, respectively. The ROx termination rate was dominated by the reaction of OH + NO₂ in the morning, and thereafter the radical self-combination gradually became the major sink of ROx in the afternoon. As the sum of the respective oxidation rates of the pollutants via reactions with oxidants, ~~t~~The atmospheric oxidation capacity was evaluated, with a peak of ~~0.75 x 10⁸ molecules cm⁻³ s⁻¹~~ 11.8 ppb h⁻¹ around noontime. The ratio of $P(O_3)$ to AOC$_{VOCs}$, which indicates the O₃ production from VOCs oxidation, trended to increase and then decrease as the NO concentration increased. Additionally, the maximum of the ratios existed when the NO concentration was approximately 1 ppb, with a median of about 2, indicating that the yield of ozone production from

34 VOCs oxidation was about 2 in this campaign.A strong positive correlation between O$_3$ formation rate and atmospheric

35 oxidation capacity was achieved, illustrating the atmospheric oxidation capacity was the potential tracer to indicate the

36 secondary pollution.

37

38   **1 Introduction**

39   Severe ambient ozone (O_3) pollution is one of China's most significant environmental challenges, especially in urban areas

40   (Shu et al., 2020; Li et al., 2019; Wang et al., 2020; Ma et al., 2019b; Wang et al., 2017). Despite the reduction in emissions of

41   O_3 precursors, O_3 concentration is increasing, especially in urban cities. The O_3 average trends for the focus megacity clusters

42   are 3.1 ppb a^{-1}, 2.3 ppb a^{-1}, 0.56 ppb a^{-1}, and 1.6 ppb a^{-1} for North China Plain (NCP), Yangtze River Delta (YRD), Pearl River

43   Delta (PRD), and Szechwan Basin (SCB), respectively (Li et al., 2019). The nonlinearity between O_3 and precursors illustrates

44   that it is necessary to explore the cause of O_3 production. The tropospheric O_3 is only generated in the photolysis of nitrogen

45   dioxide (NO_2), produced as the by-product within the radical cycling. Thus, the investigation of radical chemistry is critical to

46   controlling secondary pollution.

47   Hydroxyl radicals (OH), the dominant oxidant, control the atmospheric oxidation capacity (AOC) in the troposphere. The

48   OH radicals convert primary pollutants to secondary pollutants and are simultaneously transformed into peroxy radicals (HO_2

49   and RO_2). Within the interconvert of ROx (= OH, HO_2, and RO_2), secondary pollutants are generated, and thus the further

50   exploration of radical chemistry is significant. The radical closure experiment, an effective indicator for testing our

51   understanding of radical chemistry, has been conducted since the central role of OH radicals was recognized in the 1970s (Levy,

52   1971; Hofzumahaus et al., 2009). The underestimation of OH radicals in~~at~~ environments characterized by low nitrogen oxides

53   (NO) and high volatile organic compounds (VOCs) has been identified (Lu et al., 2013; Lu et al., 2012; Tan et al., 2017; Tan

54   et al., 2019; Yang et al., 2021; Hofzumahaus et al., 2009; Lelieveld et al., 2008; Whalley et al., 2011). New radical mechanisms

55   involving unclassical OH regeneration have been proposed, including Leuven Isoprene Mechanism (LIM) and X mechanism

56   (Peeters and Muller, 2010; Peeters et al., 2014; Peeters et al., 2009; Hofzumahaus et al., 2009). The LIM has~~ ~~ been

57   incooperated into the current mechanism and is still insufficient~~been cooperated with the current mechanism and is still not~~

58   ~~sufficient~~ to explain the OH missing sources. The X mechanism was identified several times, but the amount of the numerical

59   species, X, varied in different environments, and the nature of X is unknown (Hofzumahaus et al., 2009; Lu et al., 2013; Lu et

60   al., 2012; Tan et al., 2017; Tan et al., 2019; Yang et al., 2021). Therefore, further exploration of radical regeneration sources is

61   necessary.

62   ~~Owing~~ Due to the strong photochemistry influenced by high temperatures, high O_3 pollution appeared to occur in YRD and

63   PRD, especially in PRD (Ma et al., 2019b; Wang et al., 2017). Radicals, the dominant oxidant in the troposphere, ha~~s~~ve been

64   measured during warm seasons in NCP (Yufa 2006, Wangdu 2014, and Beijing 2016), YRD (Taizhou 2018), SCB (Chengdu

65   2019), and PRD (Backgarden 2006, and Heshan 2014) in China (Lu et al., 2013; Lu et al., 2012; Tan et al., 2017; Tan et al.,

66   2019; Yang et al., 2021; Tan et al., 2021). The radical observations in PRD, where the cities are suffering from severe O_3

67   pollution, have not been conducted since 2014, and thus the oxidation capacity here has not been clear in recent years.

68   Therefore, we carried out a continuous comprehensive field campaign (STudy of the Ozone foRmation Mechanism - STORM)

69 involving radical observations in Shenzhen, one of the megacities in PRD, in autumn 2018. Overall, the following will be

70 reported in this study.

(1) The observed ~~OH and HO₂~~ radical concentrations~~s~~, and the comparison between the radical observ~~ationsed~~ and

72 simulations~~modeled radical concentrations~~.

73 (2) The exploration of the unclassical OH regeneration sources based on the experimental budget.

74 (3) The sources and sinks of radicals.

75 (4) The evaluation of ~~AOC~~the atmospheric oxidation capacity ~~and the quantitative relationship between O₃ formation and~~

76 ~~AOC~~.

2 Methodology

2.1 Measurement site and instrumentation

79 The STORM campaign was conducted from September to October 2018 in Peking University Shenzhen Graduate School

80 (22.60 deg N, 113.97 deg E~~22°60 N, 113°97 E~~), in the west of Shenzhen, Guangdong province. As shown in Fig. 1, this site,

81 which belongs to the urban site, ~~was~~ is located in the university town, ~~which was~~and is surrounded by residential and

82 commercial areas. The northwest of the site is close to the Shenzhen Wildlife Park, and the northeast is close to the Xili Golf

83 Club (Yu et al., 2020). The Tanglang Mountain Park with active biogenic emissions is located about 1 km southeast of the site.

84 Overall, this site has no significant local pollution sources nearby, but can represent the urban pollution characteristics (Huang

85 et al., 2012b; Huang et al., 2012a; Gao et al., 2018).

87 **Figure 1: Geographical location and surrounding environmental conditions of the measurement site in STORM campaign (The**
88 **maps are from https://map.baidu.com).**

89 Most instruments were set up on the top of a four-story academic building (about 20 m). Besides HOx radicals measured by

90 the Peking University Laser-Induced Fluorescence system (PKU-LIF) (see the details in Sect. 2.2), a comprehensive set of

91 trace gases was conducted to support the exploration of the radical chemistry, including meteorological parameters

92 (temperature, pressure, relative humidity), photolysis frequency, OH reactivity (k_{OH}) and the trace gases (NO, NO$_2$, O$_3$, VOCs,

93 etc.). k_{OH} was measured by the laser flash photolysis-laser induced fluorescence (LP-LIF) system. Most of the inorganic trace

94 gases (O$_3$, CO, NO, NO$_2$, and SO$_2$) were simultaneously measured by two sets of instruments, and good agreement was

95 achieved within the uncertainty. VOCs (aldehydes, alkenes, aromatics, isoprene, and oxygenated VOCs (OVOCs)) were

96 measured using a gas chromatograph following a mass spectrometer (GC-MS). In addition, HONO and HCHO were measured

97 as well. Table S1 in the Supplementary Information describes the experimental details of the meteorological and chemical

98 parameters during this campaign.

99 **2.2 The OH and HO$_2$ measurements**

100 The OH and HO$_2$ radicals were measured by Peking University laser-induced fluorescence system (PKU-LIF) based on the

101 fluorescence assay by gas expansion (FAGE) technique. The principle has been reported in previous studies, only a brief

102 description of the instrument is presented here. Further detailed information on the instrument can be found in previous studies

103 (Heard and Pilling, 2003; Fuchs et al., 2008; Holland et al., 1995; Hofzumahaus et al., 1996; Fuchs et al., 2011).

104 In principle, OH resonance fluorescence is released in the OH excitation by a 308 nm pulsed laser, and then OH radicals are

105 detected directly. HO$_2$ radicals are converted into OH via NO, and then they are detected. The system contains a laser module

106 and a detection module. Ambient air was drawn into two independent, parallel, low-pressure (3.5 mBar) cells through two

107 parallel nozzles with 0.4 mm diameter pinhole. The OH radicals are excited into resonance fluorescence in the OH detection

108 cell and detected by micro-channel plate detectors (MCP). In the HO$_2$ detection cell, NO is injected and converts HO$_2$ to OH

109 radicals, which then are excited by the laser and release resonance fluorescence. Besides, an OH reference cell in which a large

110 OH concentration is generated by pyrolysis of water vapor on a hot filament is applied to automatically correct the laser

111 wavelength.

112 Owing to the failure of the reference cell in this study, the NO mixing ratios injected into the HO$_2$ cell were set to be higher

113 than that in other campaigns in China because the HO$_2$ cell needed to be used as a reference cell to correct laser wavelength.

114 In this campaign, NO mixing ratios were switched between 25 ppm (low NO mode) and 50 ppm (high NO mode). We

115 calculated the HO$_2$ conversion rates under the two different NO concentrations by calibrating the PKU-LIF system. HO$_2$

116 conversion rates in low NO mode ranged within 80%-95%, while those in high NO mode were over 100%, demonstrating that

117 the HO$_2$ measurement was affected by RO$_2$ radicals. Prior studies have reported the relative detection sensitivities (α_{RO_2}) for

118 the major RO$_2$ species, mainly from alkenes, isoprene and aromatics, when the HO$_2$ conversion rate was over 100% (Fuchs et

119 al., 2011; Lu et al., 2012; Lu et al., 2013). Therefore, only the HO$_2$ observations in high NO mode were chosen and they were

120 denoted as [HO$_2^*$], which was the sum of the true HO$_2$ concentration and a systematic bias from the mixture of RO$_2$ species i

121 which were detected with different relative sensitivities $\alpha_{RO_2}^i$, as shown in Eq. (1) (Lu et al., 2012). The true HO$_2$ concentration

122 was difficult to calculated because the RO$_2$ concentration measurements and their speciation were not available. Herein, we

123 simulated the HO_2 and HO_2^* concentrations by the model. The interference from RO_2 radicals was estimated to be the

124 difference between the modeled HO_2 and HO_2^* concentrations. ~~Here, NO mixing ratios were switched between 10 ppm and~~

125 ~~20 ppm. There was no obvious difference in HO_2 signals under the above two NO mixing ratios, indicating that the interference~~

126 ~~of RO_2 to HO_2 measurements was negligible despite the higher NO mixing ratio than other campaigns in China.~~

127 $$[HO_2^*] = [HO_2] + \sum(\alpha_{RO_2}^i \times [RO_2]_i) \tag{1}$$

128 Additionally, prior studies reported that OH measurement might be affected by the potential interference, when the sampled

129 air contained ozone, alkenes and BVOCs (Mao et al., 2012; Fuchs et al., 2016; Novelli et al., 2014), indicating the

130 environmental conditions are important to the production of interference. The pre-injector is usually used to test the potential

131 OH interference, and has been applied to our PKU-LIF system to quantify the possible interferences for several campaigns,

132 including the campaigns conducted in Wangdu, Heshan, Huairou, Taizhou and Chengdu sites (Tan et al., 2017; Tan et al., 2019;

133 Tan et al., 2018; Yang et al., 2021). No significant internal interference was found in the prior studies, demonstrating the

134 accuracy of the PKU-LIF system has been determined for several times. Moreover, to further explore the potential interference

135 in this campaign, we compared the major environmental conditions, especially O_3, alkenes and isoprene, between Shenzhen

136 and Wangdu sites, as shown in the Supplementary Information. The environmental condition in Shenzhen was less conducive

137 to generating interference than that in Wangdu, and the details were presented in the Supplementary Information. Therefore, it

138 is not expected that the OH measurements in this campaign were affected by the internal interference. Overall, the measurement

139 uncertainties of OH and HO_2^* radicals were 11% and 15%, respectively, as shown in Table S1 in the Supplementary

140 Information.

141

142 **2.3 Closure experiment**

143 As an effective tool to explore the atmospheric radical chemistry, the radical closure experiment can investigate the state-of-

144 the-art chemical mechanism because of the extremely short lifetime of radicals (Stone et al., 2012; Lu et al., 2019). A zero-

145 dimensional box model was used to conduct the radical closure experiment, and the overall framework was reported by Lu et

146 al. (2019). In this work, we conducted the radical closure experiment based on the Regional Atmospheric Chemical Mechanism

147 updated with the ~~lasted~~ latest isoprene chemistry (RACM2-LIM1), as Tan et al. (2017) described in detail. The model was

148 constrained to the measured meteorological, photolysis frequency, and the critical chemical parameters (CO, NO, NO_2, VOCs,

149 *etc.*). The H_2 and CH_4 mixing ratios were set to 550 ppb and 1900 ppb, respectively. The model was operated in time-dependent

150 mode with a 5-min time resolution, and a 2-d spin-up time was to make the unconstrained species approach the steady state

151 relative to the constrained species~~used to reach steady-state conditions for long-lived species~~.

152 As Lu et al. (2012) described, there are two types of radical closure experiment. One is the comparison of observed and

153 modeled radical concentrations, and the other is the comparison of radical production and destruction rates. The most

154 significant difference between the above is that the latter is conducted with the observed radical concentrations and k_{OH}

155 constrained. The comparison of radical production and destruction rates, also called radical experimental budget, can test the

156 accuracy of the state-of-the-art chemistry mechanisms based on the equivalent relationship between the radical production and

157 destruction rates. The production rates of OH, HO_2, and RO_2 radicals are quantified from all the known sources. The destruction

158 rates of HO_2 and RO_2 radicals are the sum of the known sources. The OH destruction rate can be directly calculated as the

159 product of the observed OH concentrations and the observed k_{OH} (Tan et al., 2019; Yang et al., 2021). The OH destruction rate

160 is the total sinks of OH radicals because of the direct k_{OH} observation, and thus the discrepancy between the OH destruction

161 and production rates denotes the missing OH sources. The detailed reactions and the reaction rate constants related to OH,

162 HO_2, and RO_2 radicals can be found in Tan et al. (2019) and Yang et al. (2021).

163 **2.4 AOC evaluation**

164 The life time of the trace gases is controlled not only by the oxidant concentration but also by its second-order rate constant,

165 so the atmospheric oxidation capacity (AOC) proposed by Geyer et al. (2001) is most suitable to evaluate the relative

166 importance of each oxidant (Elshorbany et al., 2009). AOC is the core driving force of complex air pollution, and determines

167 the removal rate of trace gases and the production rates of secondary pollutants (Liu et al., 2021). As an effective indicator for

168 atmospheric oxidation intensity, the evaluation of AOC can provide crucial information on the atmospheric composition of

169 harmful and climate forcing species (Elshorbany et al., 2009). AOC is defined as the sum of the respective oxidation rates of

170 the pollutants via reactions with oxidants (Elshorbany et al., 2009; Geyer et al., 2001; Zhu et al., 2020). According to the

171 definition of AOC, it can be calculated by the Eq. (~~1~~2).

172 $$AOC = \sum_i k_{Y_i}[Y_i][X] \tag{2~~1~~}$$

173 where Y_i are the pollutants (CO, ~~NO, NO₂~~CH₄, and VOCs), X are the main atmospheric oxidants (OH, O_3, NO_3), and k_{Y_i}

174 is the bi-molecular rate constant for the reaction of Y_i with X. AOC includes all combination of pollutants Y and oxidants X.

175 The higher AOC, the higher removal rate of the most pollutants, and thus the higher production rate of secondary pollutants

176 (Yang et al., 2020a). Simultaneous measurements of OH and the key trace gases are available in the study. NO_3 concentration

177 could be simulated by the box model with the observed parameters constrained.

178 **3. Results**

179 **3.1 Meteorological and chemical conditions**

180 Figure 2 gives an overview of the meteorological and chemical parameters from 05 October to 28 October 2018, when OH

181 and HO_2 radicals were measured. The diurnal variations of the temperature (T), relative humidity (RH), $j(O^1D)$, and $j(NO_2)$

182 followed a regular pattern from day to day. The overall meteorological conditions were characterized by high temperature

183 (about 20~30 ℃), high relative humidity (60~80%), and intensive radiation with $j(O^1D)$ up to 2.0×10^{-5} s^{-1} and $j(NO_2)$ up to

184 6.0×10^{-3} s^{-1}. The relative humidity and photolysis-frequency in this autumn campaign were similar to those in the summer

185 campaign conducted at Chengdu site (Yang et al., 2021). The temperature in this campaign was lower than that at Chengdu

186 site, but similar to that in the autumn campaign at Heshan site located in PRD as well (Tan et al., 2019; Yang et al., 2021).

187   The concentration of CO showed weak diurnal variation, indicating there was the non-obvious accumulation of

188 anthropogenic emissions on a regional scale. NO concentration peaked at 12 ppb during morning rush hour when the traffic

189 emission was severe, and thereafter, O_3 concentration started to increase with the decreasing of NO concentration. The maxima

190 of O_3 hourly concentration were high up to 120 ppb. According to the updated National Ambient Air Quality Standard of China

191 (GB3095-2012), O_3 concentration exceeded the Class-II limit values (hourly averaged limit 93 ppb) on several days (6, 7, 8,

192 and 26 October) when the environmental condition was characterized by high temperature and low relative humidity. NO_2

193 concentration was high at night because of the titration effect of O_3 with NO.

194   Along with the high O_3 concentration on 6, 7, 8, and 26 October, high HCHO concentration was also recorded during the

195 corresponding periods, indicating HCHO was mainly produced as secondary pollutions because of the active photochemistry

196 in this campaign. Isoprene, mostly derived from biogenic emissions and mainly affected by temperature, peaked around

197 noontime. Tan et al. (2019) reported the median concentration of HCHO and isoprene concentrations were 6.8 ppb and 0.6 ppb

198 during 12:00-18:00 at Heshan site. Similarly, the median concentration of HCHO and isoprene concentrations in this study

199 were 4.9 ppb and 0.4 ppb during the corresponding periods, respectively. As a proxy for traffic intensity, the toluene to benzene

200 ratio (T/B), which is below 2, means the traffic emissions are the major sources of VOCs (Brocco et al., 1997). The T/B

201 gradually dropped from 07:00 until it reached the minimum value at 09:00, indicating traffic emission contributed more to

202 VOCs during morning rush hour than during other periods. However, the T/B, which varied within a range of 7-12, was above

203 2, and thus VOCs emission during this campaign was mainly from other sectors such as those involving solvent evaporation.

204
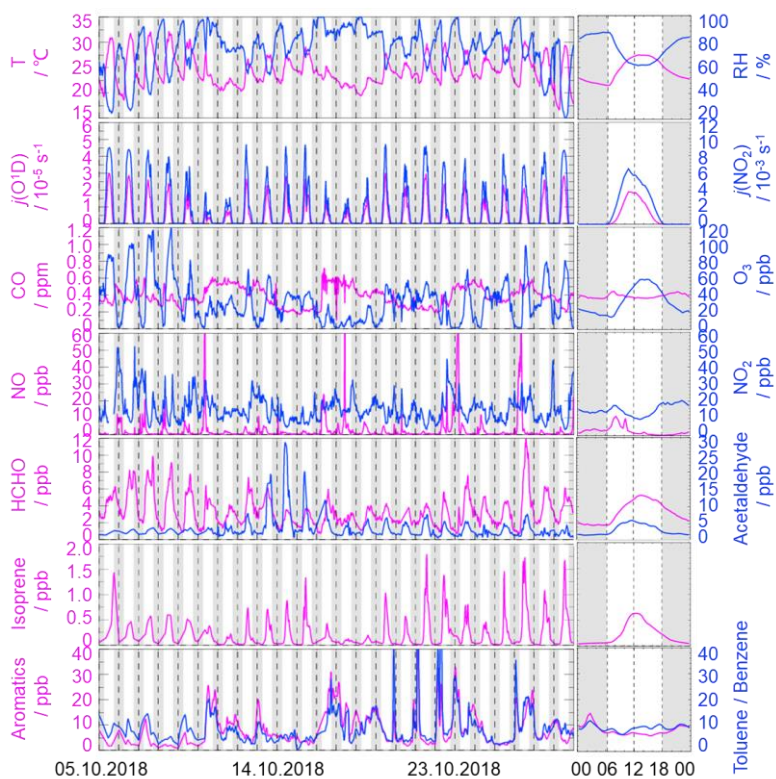
Figure 2: Timeseries and diurnal profiles of the observed meteorological and chemical parameters in STORM campaign. The grey areas denote nighttime.

Moreover, we compared the environmental conditions between the Backgarden (rural site), Heshan (suburban site), and Shenzhen (urban site) campaigns conducted in PRD in Table S3 in the Supplementary Information. No significant discrepancy in temperature was found in the Shenzhen and Heshan campaigns, which were both conducted in autumn. The temperature in the Backgarden campaign conducted in summer was higher than those in Shenzhen and Heshan. The relative humidity in Shenzhen and Backgarden was higher than that in Heshan. Compared to the chemical conditions in the Heshan campaign conducted in autumn as well, the concentrations of CO, NO, NO_2, HONO, alkenes, aromatics, and HCHO in Shenzhen were lower, which might be because there were no significant local pollution sources nearby in the Shenzhen site although it was an urban site. However, the concentration of O_3 which is the typical secondary pollutant in Shenzhen was higher than that in Heshan. Compared to the environmental conditions in Heshan, the higher O_3 concentration in Shenzhen might benefit from the weather condition which was characterized by the stronger solar radiation and slightly higher temperatures.

3.2 Observed and modeled OH and HO$_2$ radicals

The OH and HO$_2$ radicals were measured during 05-28 October 2018. The timeseries of the observed and modeled HOx concentrations are displayed in Fig. S1 (a and ba-b) in the Supplementary Information. Data gaps were caused by the rain,

220 calibration, and maintenance. The daily maxima of the observed OH and HO$_2^*$~~HO$_2$~~ concentrations varied in the range of (2-

221 9) × 10^6 cm^{-3} and (2-14) × 10^8 cm^{-3}, respectively. As in previous campaigns, the largest OH concentrations appeared around

222 noontime and showed a high correlation with j(O^{1}D), a proxy for the solar UV radiation driving much of the primary radical

223 production (Tan et al., 2019).

224 Figure 3 (a-b) shows the diurnal profiles of the observed and modeled HOx concentrations ~~(a and b)~~. The HOx radicals

225 showed similar diurnal behavior to those reported in other campaigns (Ma et al., 2019a; Tan et al., 2017; Tan et al., 2019; Tan

226 et al., 2018; Yang et al., 2021). The observed OH and HO$_2^*$~~HO$_2$~~ concentration~~s~~ reached a maximum around 12:00 and 13:30,

227 respectively. The diurnal maxim~~aum~~ of the observed and modeled OH concentration~~s~~ were~~was~~ 4.5 × 10^6 cm^{-3} and 3.5 × 10^6

228 cm^{-3}. Compared to the other campaigns conducted in PRD (Backgarden and Heshan), the diurnal maximum of the observed

229 OH concentration in Shenzhen was equal to that observed in Heshan, and much lower than that observed in Backgarden where

230 the observed OH concentration was nearly 15 × 10^6 cm^{-3} (Hofzumahaus et al., 2009; Tan et al., 2019). The higher OH

231 concentration in Backgarden site was closely correlated to the stronger solar radiation, as shown in Table S3, in the

232 Supplementary Information. ~~There was an agreement between the diurnal profiles of t~~The diurnal observed and modeled OH

233 concentrations agreed within their 1-σ uncertainties of measurement and simulation ~~errors of~~ (11% and 40%)~~, respectively~~.

234 However, when the NO mixing ratio (Fig. 2) dropped from 10:00 gradually, ~~A~~a systematic difference existed~~, with the~~

235 ~~decreasing of NO concentration~~ with the observed OH concentration being about 1×10^6 cm^{-3} higher than the modeled OH

236 concentration. ~~The model could reproduce the observed OH concentrations well only in the early morning before 10:00.~~

237 ~~However, the model would underestimate the observed OH concentration after 10:00 when NO concentration dropped 2 ppb.~~

238 The OH concentrations observed in the environments with low NO levels were underestimated by the state-of-the-art models

239 at Backgarden (summer) and Heshan (autumn) sites in PRD as well, and the OH underestimation was identified to be universal

240 at low NO conditions in China (Lu et al., 2013; Lu et al., 2012; Ma et al., 2019a; Tan et al., 2017; Yang et al., 2021). The

241 reasons on OH underestimation was further discussed in Section 4.1.
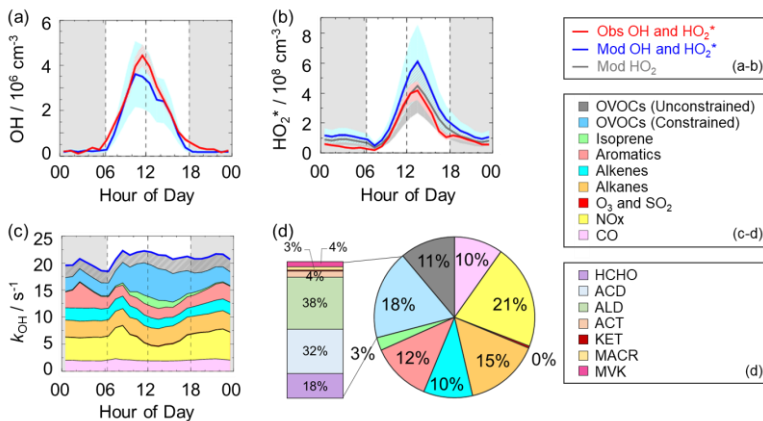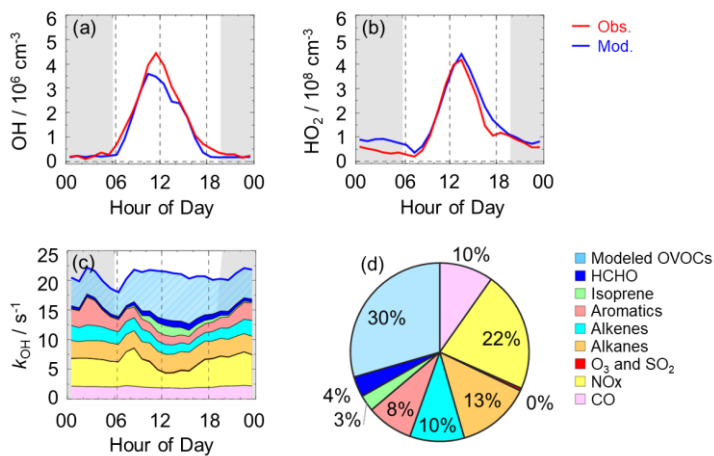
Figure 3: **(a-b)** The diurnal profiles of the observed and modeled OH~~, (a) and~~ HO$_2^*$ ~~and HO$_2$~~HO$_2$ **(b)** concentrations~~, (c) the~~ The diurnal profiles of the modeled k_{OH} ~~(c),~~ **(d)**~~and the~~ The composition of the modeled k_{OH} **(d)**. The red areas in (a-b) denote 1-σ uncertainties of the observed OH and HO$_2^*$ concentrations. The blue areas in (a-b) denote 1-σ uncertainties of the modeled OH and HO$_2^*$ concentrations, and the grey area in (b) denotes 1-σ uncertainties of the modeled HO$_2$ concentrations. The grey areas in (a-c) denote nighttime. ACD denotes acetaldehydes. ALD denotes the C3 and higher aldehydes. ACT and KET denote acetone and ketones. MACR and MVK denote methacrolein and methyl vinyl ketone.

The diurnal maximum of the observed HO$_2^*$, the modeled HO$_2^*$ and the modeled HO$_2$ concentrations were 4.2×10^8 cm^{-3}, 6.1×10^8 cm^{-3}, and 4.4×10^8 cm^{-3}, respectively. The difference between the modeled HO$_2^*$ and HO$_2$ concentrations can be considered a modeled HO$_2$ interference from RO$_2$ (Lu et al., 2012). The RO$_2$ interference was small in the morning, while it became larger in the afternoon. It ranged within 23%-28% during the daytime (08:00-17:00), which was comparable with those in the Backgarden and Yufa sites in China, Borneo rainforest in Malaysia (OP3 campaign, aircraft), and UK (RONOCO campaign, aircraft) (Lu et al., 2012; Lu et al., 2013; Jones et al., 2011; Stone et al., 2014). The observed HO$_2^*$ was

overestimated by the model, indicating the HO$_2$ heterogeneous uptake might have a significant impact during this campaign. The diurnal maximum of HO$_2$* concentration observed in Shenzhen was much lower than those observed in the Yufa and Backgarden sites (Hofzumahaus et al., 2009; Lu et al., 2012; Lu et al., 2013). ~~The diurnal maximum of the observed HO$_2$ concentration was 4.5 × 10^8 cm^{-3}, and the modeled HO$_2$ concentration could match well with the observed HO$_2$ concentration within the uncertainties, indicating the HO$_2$ heterogeneous uptake on HO$_2$ chemistry was negligible.~~ The high modeled HO$_2$/OH ratio ~~The observed HO$_2$ concentration~~ around noontime (11:00-15:00), which was about 138, was found in this campaign ~~was high, thereby yielding a mean HO$_2$ to OH ratio (HO$_2$/OH) of about 112~~, which was higher than those ~~similar to that at~~ in the Backgarden and Chengdu site~~s and was higher than that at Chengdu site~~ (Yang et al., 2021; Hofzumahaus et al., 2009). High HO$_2$/OH ratio is normally found only in clean air at low concentrations of NOx (Hofzumahaus et al., 2009; Stevens et al., 1997). ~~The modeled HO$_2$/OH ratio was about 138. Prior studies indicated that the measured HO$_2$/OH ratios were agreed well with the simulations under polluted conditions, but under clean conditions, the measured ratios were lower than simulated (Stevens et al., 1997). The comparison of the measured HO$_2$/OH ratio and the modeled HO$_2$/OH ratio in this campaign indicated the pollution was not severe during the observation period.~~ As an indicator that can reflect the interconversion reaction between ~~OH and~~ HO$_2$ and OH, the conversion efficiency in this campaign ~~was equal to that at Backgarden site and~~ was slightly slower than that in the Backgarden and ~~at~~ Chengdu site~~s~~.

3.3 ~~Modeled k_{OH}~~ OH reactivity

k_{OH} is the pseudo-first-order loss rate coefficient of OH radicals, and it is equivalent to the reciprocal OH lifetime (Fuchs et al., 2017; Lou et al., 2010; Yang et al., 2019). In this campaign, k_{OH} was measured only for several days (05-19 October 2018) by the LIP-LIF system, which has been reported in the previous study (Liu et al., 2019). The timeseries of the observed and modeled k_{OH} during 05-19 October 2018 are presented in Fig. S2 in the Supplementary Information. A good agreement between the observed k_{OH} and modeled k_{OH} within the uncertainties was achieved, and thus the model can be believed to reproduce the observed k_{OH} values within the whole campaign ~~k_{OH} was not measured continuously, so we only showed the timeseries of modeled values in Fig. S1 (c) in the Supplementary Information, the diurnal profile of the modeled k_{OH} in Fig. 3 (c), and the composition of k_{OH} in Fig. 3 (d)~~. Moreover, to reflect the k_{OH} in the whole campaign, the modeled values were shown in the k_{OH} diurnal profiles (Fig. 3c) during 05-28 October 2018. The modeled k_{OH} showed weak diurnal variation and varied from 18 s^{-1} to 22 s^{-1}. Compared to the k_{OH} variation in Shenzhen, the k_{OH} observed in Backgarden and Heshan sites in PRD showed a stronger diurnal variation, with a minimum value at around noontime and a maximum value at daybreak. The k_{OH} ranges in Backgarden and Heshan sites were 20-50 s^{-1} and 22-32 s^{-1} (Lou et al., 2010; Tan et al., 2019). Similar with the good agreement between the observed and modeled k_{OH} during the several days in Shenzhen, the observed k_{OH} in Backgarden was matched well with the modeled k_{OH} which has included the OVOCs reactivity. In terms of the k_{OH} in Heshan, Tan et al. (2019) reported that only half of the observed k_{OH} was explained by the calculated k_{OH} which was calculated from the measured trace gas

287 concentrations. The missing k_{OH} in Heshan was likely caused by unmeasured VOCs, demonstrating the necessary to measure

288 more abundant VOCs species, especially OVOCs species.

289 As shown in Fig. 3(d), we presented the composition of modeled k_{OH}. The inorganic compounds contributed approximately

290 ~~32~~31% to k_{OH}, in which the CO and NOx reactivity accounted for 10% and ~~22~~21%, respectively. The NOx reactivity ~~is~~was

291 displayed versus time, with a maximum during the morning peak. The peak concentration during the morning peak ~~is~~ was

292 associated with traffic emissions.

293 ~~The larger fraction of k_{OH} comes from the VOCs group compared with inorganics reactivity, with a contribution of 68% to~~

294 ~~k_{OH}. OVOCs reactivity was equivalent to the other VOCs reactivity, and the contributions of them to k_{OH} were both 34%. The~~

295 ~~contribution of alkanes, alkenes, and aromatics were 13%, 10%, and 8%, respectively. The isoprene reactivity related to~~

296 ~~temperature was mainly concentrated during the daytime, whereas the aromatics reactivity at night was higher. As for OVOCs~~

297 ~~species, about 4% of k_{OH} could be attributed to HCHO. The remaining OVOCs was attributed to the simulated species in the~~

298 ~~box model, with a contribution of up to 30% of k_{OH}. High OVOCs reactivity occurred in the afternoon, which was attributed~~

299 ~~to the strong photochemical activity during this period.~~Compared with the inorganics reactivity, the larger fraction of k_{OH} came

300 from the VOCs group, with a contribution of 69% to k_{OH}. The contribution of alkanes, alkenes, and aromatics were 15%, 10%,

301 and 12%, respectively. The isoprene reactivity related to temperature was mainly concentrated during the daytime, whereas

302 the aromatics reactivity at night was higher. As for the OVOCs species, we measured several OVOCs species, including HCHO,

303 acetaldehydes (ACD) and higher aldehydes (ALD), acetone (ACT), ketones (KET) and isoprene oxidation products (MACR

304 and MVK), so we constrained these species in the model. The constrained OVOCs species accounted for 18% in the total k_{OH},

305 where HCHO, ACD, and ALD were the major contributors, with contributions of 18%, 32%, and 38% to the constrained

306 OVOCs, respectively. The contribution of aldehydes in this study (16%) was larger than that in Beijing (Whalley et al., 2021)

307 and smaller with that in Wangdu (Fuchs et al., 2017). The remaining reactivity was attributed to the unconstrained OVOCs

308 reactivity, which came from the model-generated intermediate species (glyoxal, methylglyoxal, methyl ethyl ketone, methanol,

309 etc.), with a contribution of 11% to the total k_{OH}. Large fraction of OVOCs reactivities in k_{OH} was also found in some previous

310 studies (Lou et al., 2010; Lu et al., 2013; Fuchs et al., 2017; Whalley et al., 2021). About 50% of k_{OH} was explained by OVOCs

311 in Backgarden site, and HCHO, ACD and ALD, and oxygenated isoprene products were the most important OH reactants in

312 OVOCs, with a contribution of 30-40%, and other 10-20% came from other oxygenated compounds (ketones, dicarbonyl

313 compounds, alcohols, hydroperoxides, nitrates etc.) (Lou et al., 2010). HCHO, ACD, MVK, MVCR and glyoxal accounted for

314 one-third of the total k_{OH} in Wangdu site (Fuchs et al., 2017). The large unconstrained OVOCs reactivity indicated it is

315 necessary to measure more VOCs species in the future.

设置了格式: 字体: 10 磅
设置了格式: 字体: 10 磅
设置了格式: 字体: 10 磅
设置了格式: 字体: 10 磅
设置了格式: 字体: 10 磅
设置了格式: 字体: 10 磅
设置了格式: 字体: 10 磅
设置了格式: 字体: 10 磅
设置了格式: 字体: 10 磅
设置了格式: 字体: 10 磅
设置了格式: 字体: 10 磅
设置了格式: 字体: 六号

4. Discussion

4.1 Radical closure experiment

In this study, we conducted OH radical closure experiment which is called OH experimental budget as well. As discussed in Section 3.3, it is believed that the model can reproduce the observed k_{OH}. Herein, to conduct the OH experiment budget in the whole campaign, we used the modeled k_{OH} to calculate the OH destruction rate because the k_{OH} was only measured on several days. ~~The exploration of OH experimental budget was based on the premise that the modeled k_{OH} could matched well with the observed k_{OH} due to the lack of the continuous k_{OH} observations in this campaign. Several studies in China indicated that the modeled k_{OH} which has included OVOCs reactivity could match well with the observed k_{OH}, especially during daytime (Fuchs et al., 2017; Lou et al., 2010), but missing k_{OH} existed in some environmental conditions despite the inclusion of OVOCs (Whalley et al., 2021; Yang et al., 2017). Thus, the OH destruction rate is the lower limit due to the possible missing k_{OH} in this study, so the missing OH source, which is the difference between the OH destruction and production rates, is the lower limit as well.~~ The diurnal profiles of OH production and destruction rates, and compositions of OH production rate were displayed in Fig. 4, with maxima of 14 ppb h^{-1} and 17 ppb h^{-1} around noontime, respectively. The OH production rate from known sources is quantified from the primary sources (photolysis of HONO, photolysis of O$_3$, ozonolysis of alkenes) and secondary sources (dominated by HO$_2$ + NO, and HO$_2$ + O$_3$). The primary and secondary sources were account for 78% and 22% of the total calculated production rate, respectively. Similar with the prior studies, the largest fraction of OH production rate comes from HO$_2$ + NO, with a contribution up to 76% of the known OH production rate. The contributions of HONO and O$_3$ photolysis were 13% and 7% to the primary production rate.

The OH production rate matched well with the destruction rate only in the early morning to about 10:00. Thereafter, the OH destruction rate was larger than the production rate, which could explain the underestimation of OH concentration by the model. The discrepancy between the OH production and destruction rates was attributed the missing OH sources. The biggest additional OH source was approximately 4.6 ppb h^{-1}, which occurred at about 12:00, when the OH production and destruction rates were 11.9 ppb h^{-1} and 16.5 ppb h^{-1}, respectively. The unknown OH source ~~could explain~~accounted for about one third of the total OH production rate, indicating the exploration of missing OH source was significant to study the radical chemistry. It is noted that the OH production rate was overestimated because we used HO$_2^*$ concentrations instead of HO$_2$ concentrations here. Thus, the missing OH source was the lower limit here, demonstrating more unknown OH sources need to be further explored. Details on unknown OH sources are given below (Sect. 4.2).
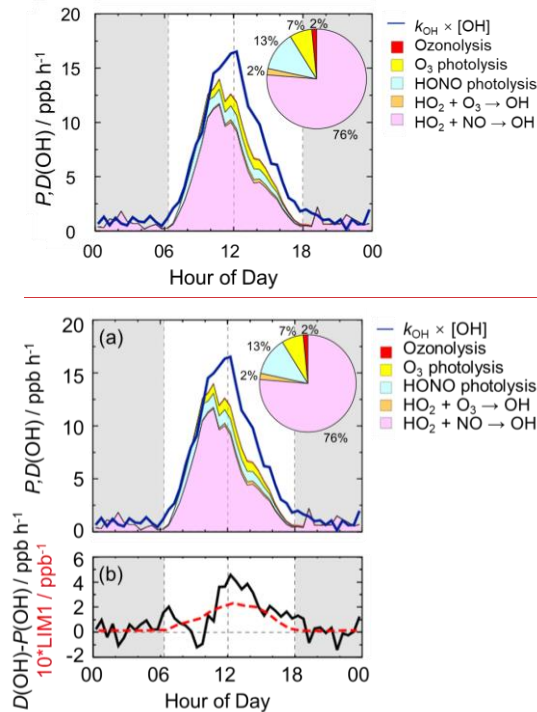
Figure 4: (a) The diurnal profiles of OH production and destruction rates and the proportions of different known sources in the calculated production rate during the daytime. The blue line denotes the OH destruction rate, and the colored areas denote the calculated OH production rates from the known sources. (b) The missing OH source which was the discrepancy between the OH destruction and production rates, and the OH production rate which was ten times the production rate derived from LIM1 mechanism. The grey areas denote nighttime.

4.2 Radical chemistry in low NO regime

4.2.1 Influencing factors of OH underestimation

As analyzed in Sect. 4.1, the underestimation of OH concentration was attributable to the missing OH source. It is necessary to explore the influencing factor for gaining further insight into the missing source. Scientists reported that more significant OH underestimation would appear with the decreasing NO concentration and increasing isoprene concentration (Lu et al., 2012; Ren et al., 2008; Hofzumahaus et al., 2009; Lelieveld et al., 2008; Whalley et al., 2011; Tan et al., 2017; Yang et al., 2021). ~~A new OH source was suggested, such as the LIM, which was proposed based on *ab inito* calculation (Peeters et al., 2014; Peeters et al., 2009). We have applied the latest LIM into the base model in this study, and Tan et al. (2017) described the modified LIM in detail. However, the model was not sufficient to explain the higher OH observations after 10:00.~~ Herein, ~~W~~we further explored the effect of NO concentration on missing OH source. NO dependence of OH and HO_2 radicals was illustrated in Fig. 5. The OH concentrations were normalized by the averaged $j(O^1D)$ to eliminate the influence of radiation on

radicals. The OH concentration showed a increasing trend with the increase of NO concentrations in low NO regime (below 1 ppb) due to the increased OH radicals from propagation via peroxy reactions with NO, and then decreased with the increase of NO concentrations in high NO regime (above 1 ppb) due to the loss by the reaction of OH with NO_2 (Ehhalt, 1999). The base model can reproduce the observed OH concentration in~~at~~ high NO regime ~~conditions (above 1 ppb)~~ and underestimate OH concentration ~~at~~ in low NO regime~~conditions (below 1 ppb)~~. As for HO_2^*~~HO_2~~ radicals, the observed and modeled HO_2^* concentrations decreased with the increase of NO concentrations. The model overestimated the observations, indicating the heterogeneous uptake might make a significant role in HO_2 sinks in this campaign~~the modeled HO_2 concentration by the base model matched well with the observed HO_2 concentration within the whole NO regime. Therefore, NO concentration played the significant role in the OH underestimation, especially under low NO regime.~~Overall, NOx (= NO + NO_2) plays a crucial role in radical chemistry due to the impact of NO on radical propagation and termination reactions.

373
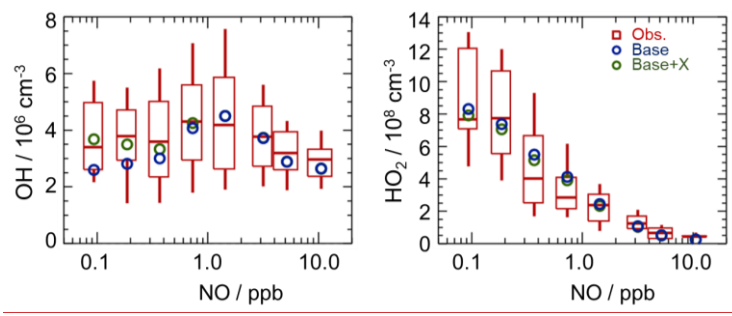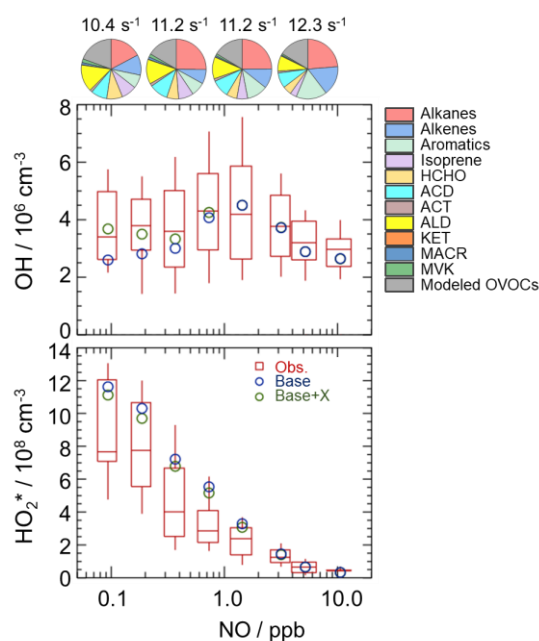
Figure 5: NO dependence of OH and ~~HO₂~~ HO₂* radicals. The red box-whisker plots give the 10%, 25%, median, 75%, and 90% of the HOx observations. The blue circles show the median values of the HOx simulations by the base model, and the green circles show the HOx simulations by the model with X mechanism. ~~The OH concentrations were normalized by the averaged *j*(O¹D) to eliminate the influence of radiation on the OH radicals.~~ Total VOCs reactivity and their organic speciation are presented by pie charts at the different NO intervals at the top. Only daytime values and NO concentration above the detection limit of the instrument were chosen. ACD and ACT denote acetaldehyde and acetone, respectively. ALD denotes the C3 and higher aldehydes. KET denotes ketones. MACR and MVK, which are both the isoprene oxidation products, denote methacrolein and methyl vinyl ketone, respectively.

设置了格式: 字体: 加粗

To further explore the influencing factors of OH underestimation, we presented the speciation VOCs reactivity under the different NO intervals, as shown in Fig. 5 and Table S4 in the Supplementary Information. The isoprene reactivity and total OVOCs reactivity (the sum of HCHO, ACD, ACT, ALD, KET, MACR, MVK and the modeled OVOCs) increased with the decrease of NO concentrations, while the anthropogenic VOCs reactivity (alkanes, alkenes and aromatics) was higher in high NO regime. Additionally, the O_3 concentration in low NO regime was significantly higher than those in high NO regime, and the temperature was slightly higher in low NO regime, demonstrating the photochemistry was more active in low NO regime in this campaign. Overall, the photochemistry and composition of VOCs reactivity, especially the isoprene and OVOCs species (mainly ACD, ACT and the modeled OVOCs), might closely impact the missing OH sources.

带格式的: 缩进: 首行缩进: 1 字符, 行距: 1.5 倍行距

4.2.2 Quantification of missing OH sources

Hofzumahaus et al. (2009) proposed an existence of a pathway for the regeneration of OH independent of NO, including the conversions of $RO_2 \rightarrow HO_2$ and $HO_2 \rightarrow OH$ by a numerical species called X. With a retrospective analysis, the unclassical

392 OH recycling pathway was identified to be universal at low NO conditions in China. The amount of X varies with

393 environmental conditions, and the X concentrations were 0.85 ppb, 0.4 ppb, 0.1 ppb, 0.4 ppb, and 0.25 ppb at Backgarden,

394 Yufa, Wangdu, Heshan, and Chengdu sites (Hofzumahaus et al., 2009; Lu et al., 2012; Lu et al., 2013; Tan et al., 2017; Yang

395 et al., 2021).

396 In this study, we tested this unclassical X mechanism. Good agreement between observations and simulations of ~~both~~ OH

397 ~~radicals and HO₂~~ was achieved when a constant mixing ratio of 0.1 ppb of X was added into the base model. As shown in Fig.

398 5, the model with X mechanism ~~could~~ agreed with the observed OH concentrations even at low NO conditions. Unclassical

399 OH recycling was identified again in this study. However, X is an artificial species that behaves like NO, and thus the nature

400 of X is still unknown to us. Compared to Shenzhen site, the required X concentration in the Backgarden and Heshan sites in

401 PRD were higher, which might be affected by the different air masses in the three sites. The k_{OH} in Shenzhen site was much

402 lower than those in Backgarden and Heshan sites, and the weaker diurnal variation of k_{OH} in Shenzhen was observed. Under

403 the influence of the East Asian monsoon, the prevailing wind for PRD area is mostly southerly during the summer months and

404 mostly northerly during the winter months (Fan et al., 2005; Zhang et al., 2008). The Backgarden site is located in Guangzhou,

405 and the Heshan site is located in Jiangmen. The two cities are along the north-south axis, and thus the air masses of the

406 Backgarden and Heshan sites are intimately linked with each other, while the air mass in Shenzhen is more similar to Hongkong

407 (Zhang et al., 2008). Therefore, ~~However, X is an artificial species that behaves like NO, and thus the nature of X is still~~

408 ~~unknown to us. f~~Further exploration on this unclassical OH recycling is needed to improve our understanding of radical

409 chemistry.

410 As discussed in Section 4.2.1, isoprene and OVOCs might have potential influence on the missing OH source. RO₂

411 isomerization reactions have also been shown to be of importance for the atmospheric fate of RO₂ from isoprene (Peeters et

412 al., 2009; Peeters et al., 2014). The latest isoprene isomerization mechanism, which is called LIM1, has been coupled into our

413 current base model. However, LIM1 mechanism was not included in the OH experimental budget, which was conducted with

414 the observations constrained, as shown in Section 4.1. Herein, we evaluated the contribution of LIM1 mechanism to the missing

415 OH sources, as shown in Fig. 4 (b). LIM1 mechanism can explain approximately 7% of the missing OH sources during 10:00-

416 16:00, when the missing OH production rate and the OH production rate derived from LIM1 mechanism were 2.47 ppb h⁻¹ and

417 0.17 ppb h⁻¹, respectively.

418 Additionally, prior studies also reported that OH regeneration might be achieved from the oxidation of MACR and MVK,

419 which are the major first-generated products of isoprene (Fuchs et al., 2018; Fuchs et al., 2014). As a potential explanation for

420 the high OH concentration, the impacts of MACR and MVK oxidation were evaluated here. The modification of MACR

421 oxidation scheme added the H-migration reactions of MACR oxidation products (Fuchs et al., 2014). The modification of

422 MVK oxidation scheme added the reactions of MVK oxidation products with HO₂ radicals and the H-migration reactions of

423 MVK oxidation products (Fuchs et al., 2018). As presented in Fig. S3 in the Supplementary Information, no significant of the

424   MACR and MVK oxidation schemes was found in this campaign.

425   Overall, a large part of missing OH sources was not explained by the isoprene chemistry. In the future, the impact of OVOCs

426   species which was another potential OH source on missing OH sources need to be further evaluated.

427

428   **4.3 3 Sources and sinks of ROx**

429   The detailed analysis of radical sources and sinks was crucial to exploring radical chemistry. The experimental budget for HO_2

430   and RO_2 radicals could not be conducted because RO_2 was not measured during this campaign. Herein, we showed the

431   simulated results by the base model. Figure 6 illustrates the diurnal profiles of ROx primary production rate (P(ROx)) and

432   termination rate (L(ROx)), and the contributions of different channels during the daytime.

433
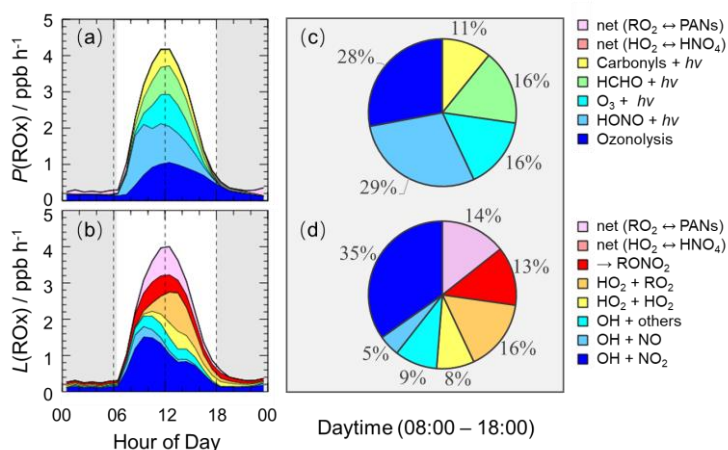
434   **Figure 6: The diurnal profiles of ROx primary production rate (a) and termination rate (b) simulated by the base model, and the**
435   **contributions of different channels to ROx primary production rate (c) and termination rate (d) during the daytime (08:00-18:00).**
436   **The grey areas denote nighttime.**

437   The ROx primary production and termination rates were basically in balance for the entire day, with maxima of 4 ppb h^{-1}

438   around noontime. The ROx primary production rate was similar to those at Heshan (4 ppb h^{-1}) and Wangdu (5 ppb h^{-1}) sites,

439   but lower than those at Backgarden (11 ppb h^{-1}), Yufa (7 ppb h^{-1}), and Chengdu (7 ppb h^{-1}) sites (Lu et al., 2013; Lu et al.,

440   2012; Tan et al., 2017; Tan et al., 2019; Yang et al., 2021). During the daytime, the main constitution of P(ROx) mainly came

441   from thewas OH and HO_2 primary production rate. HONO and O_3 photolysis mainly dominated the OH primary production

442   rate, and HCHO photolysis dominated constituted the major HO_2 primary production rate. Thus, P(ROx) was dominated by

443   the photolysis reactions, in which the photolysis of HONO, O_3, HCHO, and carbonyls accounted for 29%, 16%, 16%, and 11%

444   during the daytime, respectively. In the early morning, HONO photolysis was the most important primary source of ROx, and

445   the contribution of O_3 photolysis became progressively larger and was largest at noontime. A large discrepancy between the

446 ratio of HONO photolysis rate to O_3 photolysis rate in summer/autumn and that in winter occurs generally. The vast majority

447 of OH photolysis source is attributed to HONO photolysis in winter because of the higher HONO concentration and lower O_3

448 concentration. About half of $L(ROx)$ came from OH termination, which occurred mainly in the morning, and thereafter, radical

449 self-combination gradually became the major sink of ROx in the afternoon. $OH + NO_2$, $OH + NO$, and $OH + others$ contributed

450 35%, 5%, and 9% to $L(ROx)$, respectively. $HO_2 + HO_2$ and $HO_2 + RO_2$ accounted for 8% and 16% in $L(ROx)$.

451 **4.4 4 AOC evaluation**

452 AOC controls the abundance of precursors and the production of secondary pollutants (Yang et al., 2020b; Elshorbany et al.,

453 2009), and thus. I it is necessary to quantify AOC for understanding photochemical pollution. The AOC has been evaluated in

454 previous studies, as shown in Table 1. Overall, the AOC values in summer are higher than those in autumn and winter, and the

455 values at lower latitudes are higher than those at higher latitudes for the same rseason. The vast majority of AOC in previous

456 studies are evaluated based on the non-observed radical concentrations.

457 **Table 1: Summary of OH concentrations and AOC values reported in previous field campaigns.**

Location	Season, year	Site	Observed or non-observed of OH radicals	AOC / 10^8 molecules cm^{-3} s^{-1}	References
Beijing, China	summer, 2018	urban	non-observed values	0.89[a]	(Liu et al., 2021)
Beijing, China	summer, 2018	suburban	non-observed values	0.85[a]	(Liu et al., 2021)
Beijing, China	winter, 2018	urban	non-observed values	0.21[a]	(Liu et al., 2021)
Beijing, China	winter, 2018	suburban	non-observed values	0.16[a]	(Liu et al., 2021)
Hongkong, China	summer, 2011	suburban	non-observed values	2.04[a,b]	(Xue et al., 2016)
Santiago, Chile	summer, 2005	urban	non-observed values	3.4[a]	(Elshorbany et al., 2009)
Hong Kong, China	late summer, 2012	coastal	non-observed values	1.4[c]	(Li et al., 2018)
Hong Kong, China	autumn, 2012	coastal	non-observed values	0.62[c]	(Li et al., 2018)
Hong Kong, China	winter, 2012	coastal	non-observed values	0.41[c]	(Li et al., 2018)
Shanghai, China	summer, 2018	urban	non-observed values	1.0[c]	(Zhu et al., 2020)
Berlin, Germany	summer, 1998	suburban	non-observed values	0.14[d]	(Geyer et al., 2001)
Xianghe, China	autumn, 2019	suburban	non-observed values	0.49[c]	(Yang et al., 2020b)
Beijing, China	summer, 2014	urban	non-observed values	1.7[a]	(Feng et al., 2021)

458 Note that:

459 [a] Peak values in the diurnal profiles; [b] Values on 25 August 2021; [c] Maximum over a period of time; [d] Maximum on some day.

460 Herein, we explored the AOC in Shenzhen based on the observed radical concentrations for the first time. As illustrated in

Fig. ~~7~~ 7 (a), the diurnal profile of AOC exhibits a unimodal pattern, which is the same as the diurnal profile of OH concentration and $j(NO_2)$, with a peak around noontime. The diurnal peak of AOC was 0.75×10^8 molecules cm^{-3} s^{-1} (11.8 ppb h^{-1}). Comparatively, AOC in this study can be comparable to those evaluated in Beijing (summer, 2018) and Hong Kong (autumn, 2012) (Li et al., 2018; Liu et al., 2021), but much lower than those evaluated in Hong Kong (summer, 2011) and Santiago (summer, 2005) (Xue et al., 2016; Elshorbany et al., 2009).
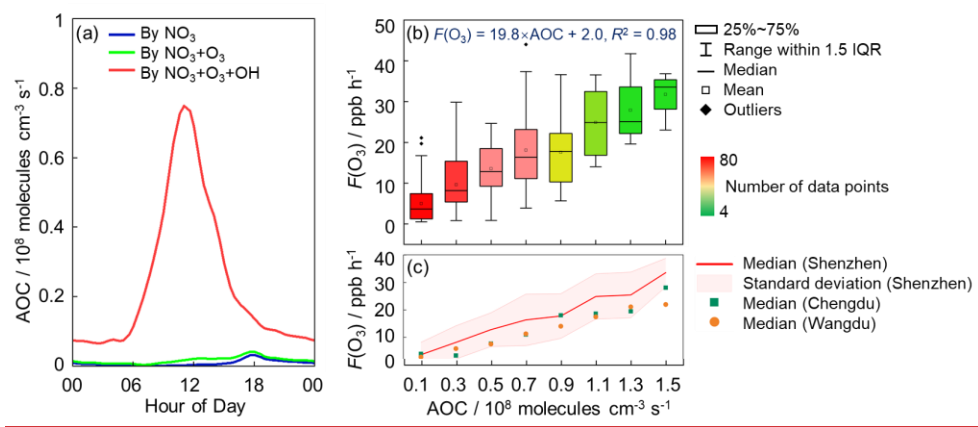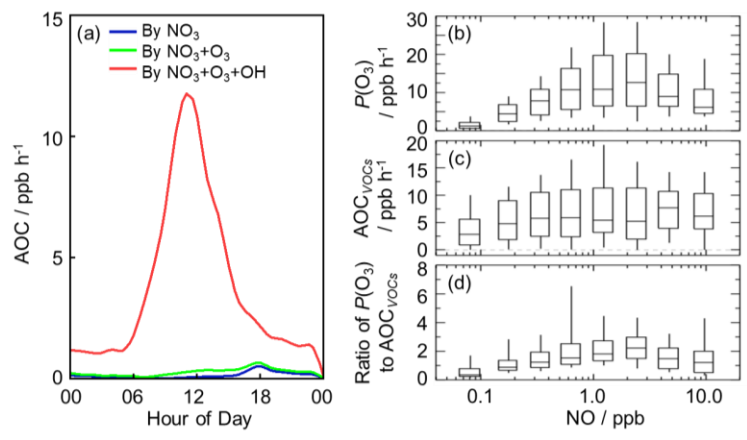
Figure ~~7~~7: (a) The diurnal profiles of AOC in this campaign. ~~(b) The correlation between $F(O_3)$ and AOC during the daytime (08:00-18:00) in this campaign, and the formula was fitted by median values. (c) The comparison of the correlations between $F(O_3)$ and AOC at this site, Wangdu site and Chengdu site.~~ **(b) NO dependence of $P(O_3)$ during the daytime. (c) NO dependence of AOC$_{VOCs}$ during the daytime, and AOC$_{VOCs}$ denotes the atmospheric oxidation capacity only from the VOCs oxidation. (d) NO dependence of the ratio of $P(O_3)$ to AOC$_{VOCs}$ during the daytime. The box-whisker plots in (b-d) give the 10%, 25%, median, 75%, and 90% $P(O_3)$, AOC$_{VOCs}$ and the ratio of $P(O_3)$ to AOC$_{VOCs}$ respectively.**

As expected, the dominant contributor to the AOC during this campaign was OH, followed by O$_3$ and NO$_3$. Figure ~~S2~~ S4

shows the fractional composition of the total AOC. The OH radical contributed about 95.7% of AOC during the daytime (08:00-18:00). O_3, as the second important oxidant, accounted for only 2.9% of AOC during the daytime. The contribution of NO_3 to AOC during the daytime can be ignored, with a contribution of 1.4%. At night, the contributions of O_3 and NO_3 to AOC were higher. OH, O_3 and NO_3 accounted for 75.7%, 6.4%, and 18% in the first half of night (18:00-24:00), and they accounted for 87.8%, 5%, and 7.3% in the second half of night (00:00-08:00).

As an indicator for secondary pollution, O_3 formation rate, $F(O_3)$, can be estimated from the production of NO_2 via the reactions of HO_2 and RO_2 with NO, as shown in Eq. (2).

$$F(O_3) = 9 \times 10^{-12}[HO_2][NO] + 9 \times 10^{-12}[RO_2][NO] \tag{2}$$

where the units of HO_2, RO_2, and NO are all cm^{-3}.

The correlation between $F(O_3)$ and AOC during the daytime (08:00-18:00) was explored, as shown in Fig. 7 (b). A strong positive correlation between $F(O_3)$ and AOC was found, indicating AOC plays a significant role in driving secondary pollution. Most data points in this campaign focused on low AOC (the median values below 0.7×10^8 molecules $cm^{-3} \cdot s^{-1}$) and low $F(O_3)$ (the median values below 17 ppb h^{-1}) regimes. The correlation between $F(O_3)$ and AOC by fitting the median was denoted by Eq. (3).

$$F(O_3) = 19.8 \times AOC + 2.0, R^2 = 0.98 \tag{3}$$

where the $F(O_3)$ and AOC units are ppb h^{-1} and 10^8 molecules $cm^{-3} \cdot s^{-1}$, respectively.

To explore the correlation between $F(O_3)$ and AOC in other regions, we have taken Wangdu and Chengdu sites as examples to demonstrate the AOC values in NCP and SCB based on the observed radical concentrations reported by Tan et al. (2017) and Yang et al. (2021) in Fig. 7 (c), respectively. Surprisingly, the relationships between $F(O_3)$ and AOC in Wangdu and Chengdu were similar to those in the Shenzhen campaign. The vast majority of data points at Wangdu and Chengdu sites were distributed within the standard deviation of Shenzhen site. The similarity of the gradients between $F(O_3)$ and AOC in different regions indicates that AOC powerfully drives the production of O_3, and the quantification of $F(O_3)$ can be achieved based on the AOC values.

As the indictor for secondary pollution, net O_3 production rate, $P(O_3)$, can be calculated from the O_3 formation rate ($F(O_3)$) and the loss rate ($L(O_3)$), as shown in Eq. (3-5) (Tan et al., 2017). The diurnal profiles of the speciation $F(O_3)$ and $L(O_3)$ were shown in Fig. S5 in the Supplementary Information. The diurnal maxima of the modeled $F(O_3)$ and $L(O_3)$ were 18.9 ppb h^{-1} and 2.8 ppb h^{-1}, with the maximum $P(O_3)$ of 16.1 ppb h^{-1} at 11:00. The modeled $P(O_3)$ was comparable to that in Wangdu site in summer and much higher than that in Beijing in winter (Tan et al., 2017; Tan et al., 2018).

$$F(O_3) = k_{HO_2+NO}[HO_2][NO] + \sum_i k_{RO_2i+NO}[RO_2]_i[NO] \tag{3}$$

$$L(O_3) = \theta j(O^1D)[O_3] + k_{O_3+OH}[O_3][OH] + k_{O_3+HO_2}[O_3][HO_2] + (\sum(k^i_{alkenes+O_3}[alkenes^i]))[O_3] \tag{4}$$

$$P(O_3) = F(O_3) - L(O_3) \tag{5}$$

where θ is the fraction of O^1D from ozone photolysis that reacts with water vapor.

Herein, we presented the NO dependence of $P(O_3)$, AOC_{VOCs}, and the ratio of $P(O_3)$ to AOC_{VOCs} in Fig. 7 (b-d), in which AOC_{VOCs} denotes the atmospheric oxidation capacity only from the VOCs oxidation. An upward trend $P(O_3)$ was presented with the increase of NO concentration when NO concentration was below 1 ppb, while a downward trend was shown with the increase of NO concentration when NO concentration was above 1 ppb. In terms of the NO dependence of AOC_{VOCs}, no significant variation was found, indicating VOCs oxidation was weakly impacted by NO concentrations in this campaign. Since AOC_{VOCs} can represent the VOCs oxidant rate, and thus the ratio of $P(O_3)$ to AOC_{VOCs} can reflect the yield of ozone production from VOCs oxidation. Similar to $P(O_3)$, the ratio increased with the increase of NO concentration when NO concentration was below 1 ppb. When NO concentration was above 1 ppb, the ratio decreased with the increase of NO concentration because NO_2 became the sink of OH radicals gradually. The maximum of the ratios existed when NO concentration was approximately 1 ppb, with a median of about 2, indicating the yield of ozone production from VOCs oxidation was about 2 in this study.

5 Conclusions

The STORM field campaign was carried out at Shenzhen site in autumn 2018, providing the continuous OH and $HO_2^*$$HO_2$ observations in PRD since the Heshan campaign in 2014. The maximum diurnal OH and $HO_2^*$$HO_2$ concentrations, measured by laser-induced fluorescence (LIF), were 4.5×10^6 cm^{-3} and 4.5×10^8 cm^{-3}, respectively. The observed OH concentration was equal to that measured at Heshan site but was lower than those measured in summer campaigns in China (Backgarden, Yufa, Wangdu, and Chengdu campaignssites).

The base model (RACM2-LIM1) could reproduce the observed OH concentration before 10:00, and thereafter, OH was underestimated by the model when NO concentration dropped to low levels. The results of the radical experimental budget indicated that OH underestimation was likely attributable to an unknown missing OH source at low NO conditions. We diagnosed the missing OH source by sensitivity runs, and unclassical OH recycling was identified again. A constant mixing ratio of the numerical species, X, equivalent to 0.1 ppb NO, was added to the base model to achieve the agreement between the modeled and observed OH concentrations. The amount of X related to the environmental conditions varied from 0.1 ppb to 0.85 ppb in China, and thus the unclassical OH recycling needs further exploration. Additionally, we found isoprene and OVOCs might closely influence the missing OH sources by comparing the composition of VOCs reactivity under the different NO intervals. Isoprene isomerization mechanism (LIM1) can explain approximately 7% of the missing OH sources, and no significant contribution of MACR and MVK oxidation was found. As another potential OH source, OVOCs species should be further explored to explain the remaining missing OH sources. As for HO_2 radicals, the overestimation of HO_2^* concentration

536 was found, indicating that HO$_2$ heterogeneous uptake might make a significant role in HO$_2$ sinks ~~good agreement between the~~

537 ~~observed and modeled HO$_2$ concentrations was achieved for the entire day during this campaign, indicating the HO$_2$~~

538 ~~heterogeneous uptake on HO$_2$ chemistry was negligible.~~

539 The quantification of production and destruction channels of ROx radicals is essential to explore the chemical processes of

540 radicals. The ROx primary production and termination rates were balanced for the entire day, with maxima of 4 ppb h^{-1}, similar

541 to those in the Heshan and Wangdu ~~campaigns~~sites. Photolysis channels dominated the ROx primary production rate. HONO,

542 O$_3$, HCHO, and carbonyls photolysis accounted for 29%, 16%, 16%, and 11% during the daytime, respectively. The most

543 fraction of ROx termination rate came from the reaction of OH + NO$_2$ in the morning. The radical self-combination gradually

544 became the major sink of ROx in the afternoon with the decreasing of NO concentrations. The reaction of OH + NO$_2$ and

545 radical self-combination accounted for 35% and 24% during the daytime, respectively.

546 ~~In this campaign, AOC exhibited well-defined diurnal patterns, with a peak of 0.75 × 10^8 molecules cm^{-3} s^{-1}. As expected,~~

547 ~~OH was the dominant oxidant accounting for 95.7% of the total AOC during the daytime. O$_3$ and NO$_3$ contributed 2.9% and~~

548 ~~1.4% to total AOC during the daytime, respectively. The gradients at Shenzhen (PRD), Wangdu (NCP), and Chengdu (SBC)~~

549 ~~sites were similar. The strong positive correlation between $F(O_3)$ and AOC makes the quantification of $F(O_3)$ achieved,~~

550 ~~indicating AOC is the core driving force for the generation of secondary pollutants.~~In this campaign, AOC exhibited well-

551 defined diurnal patterns, with a peak of 11.8 ppb h^{-1}. As expected, OH radicals, which were the dominant oxidant, accounted

552 for 95.7% of the total AOC during the daytime. O$_3$ and NO$_3$ contributed 2.9% and 1.4% to total AOC during the daytime,

553 respectively. The ratio of $P(O_3)$ to AOC$_{VOCs}$ trended to increase and then decrease as NO concentration increased,

554 demonstrating the non-linear relationship between O$_3$ production and VOCs oxidation. The maximum of the ratios existed

555 when NO concentration was approximately 1 ppb, with a median of about 2, indicating that the yield of ozone production from

556 VOCs oxidation was about 2 in this campaign.

557

558 **Data availability.** The data used in this study are available from the corresponding author upon request (k.lu@pku.edu.cn).

559

560 **Author contributions.** YH Zhang and KD Lu conceived the study. XP Yang analyzed the data and wrote the manuscript with

561 inputs from KD Lu. XP Yang, XF Ma, Y Gao contributed to the measurements of the HOx concentrations. All authors

562 contributed to the discussed results and commented on the manuscript.

563

564 **Competing interests.** The authors declare that they have no conflict of interest.

565

566 **Acknowledgment.** The authors thank the science teams of the STORM-2018 campaign. This work was supported by the

Beijing Municipal Natural Science Foundation for Distinguished Young Scholars (JQ19031),the National Research Program for Key Issue in Air Pollution Control (2019YFC0214800) , and the National Natural Science Foundation of China (Grants No. 91544225, 21522701, 91844301).

Appendix A. Supplementary data

References

Brocco, D., Fratarcangeli, R., Lepore, L., Petricca, M., and Ventrone, I.: Determination of aromatic hydrocarbons in urban air of Rome, Atmospheric Environment, 31, 557-566, 10.1016/s1352-2310(96)00226-9, 1997.

Ehhalt, D. H.: Photooxidation of trace gases in the troposphere, Physical Chemistry Chemical Physics, 1, 5401-5408, 10.1039/a905097c, 1999.

Elshorbany, Y. F., Kurtenbach, R., Wiesen, P., Lissi, E., Rubio, M., Villena, G., Gramsch, E., Rickard, A. R., Pilling, M. J., and Kleffmann, J.: Oxidation capacity of the city air of Santiago, Chile, Atmospheric Chemistry and Physics, 9, 2257-2273, 10.5194/acp-9-2257-2009, 2009.

Fan, S., Wang, A., Fan, Q., Liu, J., and Wang, B.: ATMOSPHERIC BOUNDARY LAYER CONCEPT MODEL OF THE PEARL RIVER DELTA AND ITS APPLICATION, Journal of Tropical Meteorology, 21, 286-292, 2005.

Feng, T., Zhao, S. Y., Hu, B., Bei, N. F., Zhang, X., Wu, J. R., Li, X., Liu, L., Wang, R. N., Tie, X. X., and Li, G. H.: Assessment of Atmospheric Oxidizing Capacity Over the Beijing-Tianjin-Hebei (BTH) Area, China, Journal of Geophysical Research-Atmospheres, 126, 18, 10.1029/2020jd033834, 2021.

Fuchs, H., Holland, F., and Hofzumahaus, A.: Measurement of tropospheric RO2 and HO2 radicals by a laser-induced fluorescence instrument, Review of Scientific Instruments, 79, 10.1063/1.2968712, 2008.

Fuchs, H., Bohn, B., Hofzumahaus, A., Holland, F., Lu, K. D., Nehr, S., Rohrer, F., and Wahner, A.: Detection of HO2 by laser-induced fluorescence: calibration and interferences from RO2 radicals, Atmospheric Measurement Techniques, 4, 1209-1225, 10.5194/amt-4-1209-2011, 2011.

Fuchs, H., Tan, Z., Hofzumahaus, A., Broch, S., Dorn, H.-P., Holland, F., Kuenstler, C., Gomm, S., Rohrer, F., Schrade, S., Tillmann, R., and Wahner, A.: Investigation of potential interferences in the detection of atmospheric ROx radicals by laser-induced fluorescence under dark conditions, Atmospheric Measurement Techniques, 9, 1431-1447, 10.5194/amt-9-1431-2016, 2016.

Fuchs, H., Acir, I. H., Bohn, B., Brauers, T., Dorn, H. P., Häseler, R., Hofzumahaus, A., Holland, F., Kaminski, M., Li, X., Lu, K., Lutz, A., Nehr, S., Rohrer, F., Tillmann, R., Wegener, R., and Wahner, A.: OH regeneration from methacrolein oxidation investigated in the atmosphere simulation chamber SAPHIR, Atmos. Chem. Phys., 14, 7895-7908, 10.5194/acp-14-7895-2014, 2014.

Fuchs, H., Albrecht, S., Acir, I.-H., Bohn, B., Breitenlechner, M., Dorn, H.-P., Gkatzelis, G. I., Hofzumahaus, A., Holland, F., Kaminski, M., Keutsch, F. N., Novelli, A., Reimer, D., Rohrer, F., Tillmann, R., Vereecken, L., Wegener, R., Zaytsev, A., Kiendler-Scharr, A., and Wahner, A.: Investigation of the oxidation of methyl vinyl ketone (MVK) by OH radicals in the atmospheric simulation chamber SAPHIR, Atmospheric Chemistry and Physics, 18, 8001-8016, 10.5194/acp-18-8001-2018, 2018.

Fuchs, H., Tan, Z., Lu, K., Bohn, B., Broch, S., Brown, S. S., Dong, H., Gomm, S., Haeseler, R., He, L., Hofzumahaus, A., Holland, F., Li, X., Liu, Y., Lu, S., Min, K.-E., Rohrer, F., Shao, M., Wang, B., Wang, M., Wu, Y., Zeng, L., Zhang, Y., Wahner, A., and Zhang, Y.: OH reactivity at a rural site (Wangdu) in the North China Plain: contributions from OH reactants and experimental OH budget, Atmospheric Chemistry and Physics, 17, 645-661, 10.5194/acp-17-645-2017, 2017.

Gao, M., Li, H., Li, Y., Wei, J., Sun, Y., He, L., and Huang, X.: Source characteristics of water-soluble organic matters in PM_(2.5) in the winter of Shenzhen, China Environmental Science, 38, 4017-4022, 2018.

Geyer, A., Alicke, B., Konrad, S., Schmitz, T., Stutz, J., and Platt, U.: Chemistry and oxidation capacity of the nitrate radical

in the continental boundary layer near Berlin, Journal of Geophysical Research-Atmospheres, 106, 8013-8025, 10.1029/2000jd900681, 2001.

Heard, D. E. and Pilling, M. J.: Measurement of OH and HO2 in the troposphere, Chemical Reviews, 103, 5163-5198, 10.1021/cr020522s, 2003.

Hofzumahaus, A., Aschmutat, U., Hessling, M., Holland, F., and Ehhalt, D. H.: The measurement of tropospheric OH radicals by laser-induced fluorescence spectroscopy during the POPCORN field campaign, Geophysical Research Letters, 23, 2541-2544, 10.1029/96gl02205, 1996.

Hofzumahaus, A., Rohrer, F., Lu, K., Bohn, B., Brauers, T., Chang, C.-C., Fuchs, H., Holland, F., Kita, K., Kondo, Y., Li, X., Lou, S., Shao, M., Zeng, L., Wahner, A., and Zhang, Y.: Amplified Trace Gas Removal in the Troposphere, Science, 324, 1702-1704, 10.1126/science.1164566, 2009.

Holland, F., Hessling, M., and Hofzumahaus, A.: IN-SITU MEASUREMENT OF TROPOSPHERIC OH RADICALS BY LASER-INDUCED FLUORESCENCE - A DESCRIPTION OF THE KFA INSTRUMENT, Journal of the Atmospheric Sciences, 52, 3393-3401, 10.1175/1520-0469(1995)052<3393:Ismoto>2.0.Co;2, 1995.

Huang, X.-F., Sun, T.-L., Zeng, L.-W., Yu, G.-H., and Luan, S.-J.: Black carbon aerosol characterization in a coastal city in South China using a single particle soot photometer, Atmospheric Environment, 51, 21-28, https://doi.org/10.1016/j.atmosenv.2012.01.056, 2012a.

Huang, X.-F., Chen, D.-L., Lan, Z.-J., Feng, N., He, L.-Y., Yu, G.-H., and Luan, S.-J.: Characterization of organic aerosol in fine particles in a mega-city of South China: Molecular composition, seasonal variation, and size distribution, Atmospheric Research, 114-115, 28-37, https://doi.org/10.1016/j.atmosres.2012.05.019, 2012b.

Jones, C. E., Hopkins, J. R., and Lewis, A. C.: In situ measurements of isoprene and monoterpenes within a south-east Asian tropical rainforest, Atmospheric Chemistry and Physics, 11, 6971-6984, 10.5194/acp-11-6971-2011, 2011.

Lelieveld, J., Butler, T. M., Crowley, J. N., Dillon, T. J., Fischer, H., Ganzeveld, L., Harder, H., Lawrence, M. G., Martinez, M., Taraborrelli, D., and Williams, J.: Atmospheric oxidation capacity sustained by a tropical forest, Nature, 452, 737-740, 10.1038/nature06870, 2008.

Levy, H.: NORMAL ATMOSPHERE - LARGE RADICAL AND FORMALDEHYDE CONCENTRATIONS PREDICTED, Science, 173, 141-&, 10.1126/science.173.3992.141, 1971.

Li, K., Jacob, D. J., Liao, H., Shen, L., Zhang, Q., and Bates, K. H.: Anthropogenic drivers of 2013-2017 trends in summer surface ozone in China, Proceedings of the National Academy of Sciences of the United States of America, 116, 422-427, 10.1073/pnas.1812168116, 2019.

Li, Z., Xue, L., Yang, X., Zha, Q., Tham, Y. J., Yan, C., Louie, P. K. K., Luk, C. W. Y., Wang, T., and Wang, W.: Oxidizing capacity of the rural atmosphere in Hong Kong, Southern China, Science of the Total Environment, 612, 1114-1122, 10.1016/j.scitotenv.2017.08.310, 2018.

Liu, S., Li, X., Shen, X., Zeng, L., Huang, X., Zhu, B., Lin, L., and Lou, S.: Measurement and partition analysis of atmospheric OH reactivity in autumn in Shenzhen, Acta Scientiae Circumstantiae, 39, 3600-3610, 2019.

Liu, Z., Wang, Y., Hu, B., Lu, K., Tang, G., Ji, D., Yang, X., Gao, W., Xie, Y., Liu, J., Yao, D., Yang, Y., and Zhang, Y.: Elucidating the quantitative characterization of atmospheric oxidation capacity in Beijing, China, Science of the Total Environment, 771, 10.1016/j.scitotenv.2021.145306, 2021.

Lou, S., Holland, F., Rohrer, F., Lu, K., Bohn, B., Brauers, T., Chang, C. C., Fuchs, H., Haeseler, R., Kita, K., Kondo, Y., Li, X., Shao, M., Zeng, L., Wahner, A., Zhang, Y., Wang, W., and Hofzumahaus, A.: Atmospheric OH reactivities in the Pearl River Delta - China in summer 2006: measurement and model results, Atmospheric Chemistry and Physics, 10, 11243-11260, 10.5194/acp-10-11243-2010, 2010.

Lu, K., Guo, S., Tan, Z., Wang, H., Shang, D., Liu, Y., Li, X., Wu, Z., Hu, M., and Zhang, Y.: Exploring atmospheric free-radical chemistry in China: the self-cleansing capacity and the formation of secondary air pollution, National Science Review, 6, 579-594, 10.1093/nsr/nwy073, 2019.

Lu, K. D., Hofzumahaus, A., Holland, F., Bohn, B., Brauers, T., Fuchs, H., Hu, M., Haeseler, R., Kita, K., Kondo, Y., Li, X., Lou, S. R., Oebel, A., Shao, M., Zeng, L. M., Wahner, A., Zhu, T., Zhang, Y. H., and Rohrer, F.: Missing OH source in a suburban environment near Beijing: observed and modelled OH and HO2 concentrations in summer 2006, Atmospheric

656   Chemistry and Physics, 13, 1057-1080, 10.5194/acp-13-1057-2013, 2013.

657   Lu, K. D., Rohrer, F., Holland, F., Fuchs, H., Bohn, B., Brauers, T., Chang, C. C., Haeseler, R., Hu, M., Kita, K., Kondo, Y.,

658   Li, X., Lou, S. R., Nehr, S., Shao, M., Zeng, L. M., Wahner, A., Zhang, Y. H., and Hofzumahaus, A.: Observation and modelling

659   of OH and HO2 concentrations in the Pearl River Delta 2006: a missing OH source in a VOC rich atmosphere, Atmospheric

660   Chemistry and Physics, 12, 1541-1569, 10.5194/acp-12-1541-2012, 2012.

661   Ma, X., Tan, Z., Lu, K., Yang, X., Liu, Y., Li, S., Li, X., Chen, S., Novelli, A., Cho, C., Zeng, L., Wahner, A., and Zhang, Y.:

662   Winter photochemistry in Beijing: Observation and model simulation of OH and HO2 radicals at an urban site, Science of the

663   Total Environment, 685, 85-95, 10.1016/j.scitotenv.2019.05.329, 2019a.

664   Ma, X. Y., Jia, H. L., Sha, T., An, J. L., and Tian, R.: Spatial and seasonal characteristics of particulate matter and gaseous

665   pollution in China: Implications for control policy, Environmental Pollution, 248, 421-428, 10.1016/j.envpol.2019.02.038,

666   2019b.

667   Mao, J., Ren, X., Zhang, L., Van Duin, D. M., Cohen, R. C., Park, J. H., Goldstein, A. H., Paulot, F., Beaver, M. R., Crounse,

668   J. D., Wennberg, P. O., DiGangi, J. P., Henry, S. B., Keutsch, F. N., Park, C., Schade, G. W., Wolfe, G. M., Thornton, J. A., and

669   Brune, W. H.: Insights into hydroxyl measurements and atmospheric oxidation in a California forest, Atmospheric Chemistry

670   and Physics, 12, 8009-8020, 10.5194/acp-12-8009-2012, 2012.

671   Novelli, A., Hens, K., Ernest, C. T., Kubistin, D., Regelin, E., Elste, T., Plass-Duelmer, C., Martinez, M., Lelieveld, J., and

672   Harder, H.: Characterisation of an inlet pre-injector laser-induced fluorescence instrument for the measurement of atmospheric

673   hydroxyl radicals, Atmospheric Measurement Techniques, 7, 3413-3430, 10.5194/amt-7-3413-2014, 2014.

674   Peeters, J. and Muller, J.-F.: HOx radical regeneration in isoprene oxidation via peroxy radical isomerisations. II: experimental

675   evidence and global impact, Physical Chemistry Chemical Physics, 12, 14227-14235, 10.1039/c0cp00811g, 2010.

676   Peeters, J., Nguyen, T. L., and Vereecken, L.: HOx radical regeneration in the oxidation of isoprene, Physical Chemistry

677   Chemical Physics, 11, 5935-5939, 10.1039/b908511d, 2009.

678   Peeters, J., Muller, J.-F., Stavrakou, T., and Vinh Son, N.: Hydroxyl Radical Recycling in Isoprene Oxidation Driven by

679   Hydrogen Bonding and Hydrogen Tunneling: The Upgraded LIM1 Mechanism, Journal of Physical Chemistry A, 118, 8625-

680   8643, 10.1021/jp5033146, 2014.

681   Ren, X., Olson, J. R., Crawford, J. H., Brune, W. H., Mao, J., Long, R. B., Chen, Z., Chen, G., Avery, M. A., Sachse, G. W.,

682   Barrick, J. D., Diskin, G. S., Huey, L. G., Fried, A., Cohen, R. C., Heikes, B., Wennberg, P. O., Singh, H. B., Blake, D. R., and

683   Shetter, R. E.: HOx chemistry during INTEX-A 2004: Observation, model calculation, and comparison with previous studies,

684   Journal of Geophysical Research-Atmospheres, 113, 10.1029/2007jd009166, 2008.

685   Shu, L., Wang, T. J., Han, H., Xie, M., Chen, P. L., Li, M. M., and Wu, H.: Summertime ozone pollution in the Yangtze River

686   Delta of eastern China during 2013-2017: Synoptic impacts and source apportionment, Environmental Pollution, 257,

687   10.1016/j.envpol.2019.113631, 2020.

688   Stevens, P. S., Mather, J. H., Brune, W. H., Eisele, F., Tanner, D., Jefferson, A., Cantrell, C., Shetter, R., Sewall, S., Fried, A.,

689   Henry, B., Williams, E., Baumann, K., Goldan, P., and Kuster, W.: HO2/OH and RO(2)/HO2 ratios during the Tropospheric

690   OH Photochemistry Experiment: Measurement and theory, Journal of Geophysical Research-Atmospheres, 102, 6379-6391,

691   10.1029/96jd01704, 1997.

692   Stone, D., Whalley, L. K., and Heard, D. E.: Tropospheric OH and HO2 radicals: field measurements and model comparisons,

693   Chemical Society Reviews, 41, 6348-6404, 10.1039/c2cs35140d, 2012.

694   Stone, D., Evans, M. J., Walker, H., Ingham, T., Vaughan, S., Ouyang, B., Kennedy, O. J., McLeod, M. W., Jones, R. L.,

695   Hopkins, J., Punjabi, S., Lidster, R., Hamilton, J. F., Lee, J. D., Lewis, A. C., Carpenter, L. J., Forster, G., Oram, D. E., Reeves,

696   C. E., Bauguitte, S., Morgan, W., Coe, H., Aruffo, E., Dari-Salisburgo, C., Giammaria, F., Di Carlo, P., and Heard, D. E.:

697   Radical chemistry at night: comparisons between observed and modelled HOx, NO3 and N2O5 during the RONOCO project,

698   Atmospheric Chemistry and Physics, 14, 1299-1321, 10.5194/acp-14-1299-2014, 2014.

699   Tan, Z., Ma, X., Lu, K., Jiang, M., Zou, Q., Wang, H., Zeng, L., and Zhang, Y.: Direct evidence of local photochemical

700   production driven ozone episode in Beijing: A case study, Science of the Total Environment, 800,

701   10.1016/j.scitotenv.2021.148868, 2021.

702   Tan, Z., Lu, K., Hofzumahaus, A., Fuchs, H., Bohn, B., Holland, F., Liu, Y., Rohrer, F., Shao, M., Sun, K., Wu, Y., Zeng, L.,

Zhang, Y., Zou, Q., Kiendler-Scharr, A., Wahner, A., and Zhang, Y.: Experimental budgets of OH, HO2, and RO2 radicals and implications for ozone formation in the Pearl River Delta in China 2014, Atmospheric Chemistry and Physics, 19, 7129-7150, 10.5194/acp-19-7129-2019, 2019.

Tan, Z., Fuchs, H., Lu, K., Hofzumahaus, A., Bohn, B., Broch, S., Dong, H., Gomm, S., Haeseler, R., He, L., Holland, F., Li, X., Liu, Y., Lu, S., Rohrer, F., Shao, M., Wang, B., Wang, M., Wu, Y., Zeng, L., Zhang, Y., Wahner, A., and Zhang, Y.: Radical chemistry at a rural site (Wangdu) in the North China Plain: observation and model calculations of OH, HO2 and RO2 radicals, Atmospheric Chemistry and Physics, 17, 663-690, 10.5194/acp-17-663-2017, 2017.

Tan, Z., Rohrer, F., Lu, K., Ma, X., Bohn, B., Broch, S., Dong, H., Fuchs, H., Gkatzelis, G. I., Hofzumahaus, A., Holland, F., Li, X., Liu, Y., Liu, Y., Novelli, A., Shao, M., Wang, H., Wu, Y., Zeng, L., Hu, M., Kiendler-Scharr, A., Wahner, A., and Zhang, Y.: Wintertime photochemistry in Beijing: observations of ROx radical concentrations in the North China Plain during the BEST-ONE campaign, Atmospheric Chemistry and Physics, 18, 12391-12411, 10.5194/acp-18-12391-2018, 2018.

Wang, T., Xue, L. K., Brimblecombe, P., Lam, Y. F., Li, L., and Zhang, L.: Ozone pollution in China: A review of concentrations, meteorological influences, chemical precursors, and effects, Science of the Total Environment, 575, 1582-1596, 10.1016/j.scitotenv.2016.10.081, 2017.

Wang, W., Parrish, D. D., Li, X., Shao, M., Liu, Y., Mo, Z., Lu, S., Hu, M., Fang, X., Wu, Y., Zeng, L., and Zhang, Y.: Exploring the drivers of the increased ozone production in Beijing in summertime during 2005-2016, Atmospheric Chemistry and Physics, 20, 15617-15633, 10.5194/acp-20-15617-2020, 2020.

Whalley, L. K., Edwards, P. M., Furneaux, K. L., Goddard, A., Ingham, T., Evans, M. J., Stone, D., Hopkins, J. R., Jones, C. E., Karunaharan, A., Lee, J. D., Lewis, A. C., Monks, P. S., Moller, S. J., and Heard, D. E.: Quantifying the magnitude of a missing hydroxyl radical source in a tropical rainforest, Atmospheric Chemistry and Physics, 11, 7223-7233, 10.5194/acp-11-7223-2011, 2011.

Whalley, L. K., Slater, E. J., Woodward-Massey, R., Ye, C., Lee, J. D., Squires, F., Hopkins, J. R., Dunmore, R. E., Shaw, M., Hamilton, J. F., Lewis, A. C., Mehra, A., Worrall, S. D., Bacak, A., Bannan, T. J., Coe, H., Percival, C. J., Ouyang, B., Jones, R. L., Crilley, L. R., Kramer, L. J., Bloss, W. J., Vu, T., Kotthaus, S., Grimmond, S., Sun, Y., Xu, W., Yue, S., Ren, L., Acton, W. J. F., Hewitt, C. N., Wang, X., Fu, P., and Heard, D. E.: Evaluating the sensitivity of radical chemistry and ozone formation to ambient VOCs and NOx in Beijing, Atmospheric Chemistry and Physics, 21, 2125-2147, 10.5194/acp-21-2125-2021, 2021.

Xue, L., Gu, R., Wang, T., Wang, X., Saunders, S., Blake, D., Louie, P. K. K., Luk, C. W. Y., Simpson, I., Xu, Z., Wang, Z., Gao, Y., Lee, S., Mellouki, A., and Wang, W.: Oxidative capacity and radical chemistry in the polluted atmosphere of Hong Kong and Pearl River Delta region: analysis of a severe photochemical smog episode, Atmospheric Chemistry and Physics, 16, 9891-9903, 10.5194/acp-16-9891-2016, 2016.

Yang, X., Wang, H., Tan, Z., Lu, K., and Zhang, Y.: Observations of OH Radical Reactivity in Field Studies, Acta Chimica Sinica, 77, 613-624, 10.6023/a19030094, 2019.

Yang, X., Lu, K., Ma, X., Liu, Y., Wang, H., Hu, R., Li, X., Lou, S., Chen, S., Dong, H., Wang, F., Wang, Y., Zhang, G., Li, S., Yang, S., Yang, Y., Kuang, C., Tan, Z., Chen, X., Qiu, P., Zeng, L., Xie, P., and Zhang, Y.: Observations and modeling of OH and HO2 radicals in Chengdu, China in summer 2019, The Science of the total environment, 772, 144829-144829, 10.1016/j.scitotenv.2020.144829, 2021.

Yang, Y., Wang, Y., Yao, D., Zhao, S., Yang, S., Ji, D., Sun, J., Wang, Y., Liu, Z., Hu, B., Zhang, R., and Wang, Y.: Significant decreases in the volatile organic compound concentration, atmospheric oxidation capacity and photochemical reactivity during the National Day holiday over a suburban site in the North China Plain, Environmental Pollution, 263, 114657, https://doi.org/10.1016/j.envpol.2020.114657, 2020a.

Yang, Y., Wang, Y., Yao, D., Zhao, S., Yang, S., Ji, D., Sun, J., Wang, Y., Liu, Z., Hu, B., Zhang, R., and Wang, Y.: Significant decreases in the volatile organic compound concentration, atmospheric oxidation capacity and photochemical reactivity during the National Day holiday over a suburban site in the North China Plain, Environmental Pollution, 263, 10.1016/j.envpol.2020.114657, 2020b.

Yang, Y., Shao, M., Kessel, S., Li, Y., Lu, K., Lu, S., Williams, J., Zhang, Y., Zeng, L., Noelscher, A. C., Wu, Y., Wang, X., and Zheng, J.: How the OH reactivity affects the ozone production efficiency: case studies in Beijing and Heshan, China, Atmospheric Chemistry and Physics, 17, 7127-7142, 10.5194/acp-17-7127-2017, 2017.

Yu, D., Tan, Z., Lu, K., Ma, X., Li, X., Chen, S., Zhu, B., Lin, L., Li, Y., Qiu, P., Yang, X., Liu, Y., Wang, H., He, L., Huang, X., and Zhang, Y.: An explicit study of local ozone budget and NOx-VOCs sensitivity in Shenzhen China, Atmospheric Environment, 224, 117304, https://doi.org/10.1016/j.atmosenv.2020.117304, 2020.

Zhang, Y. H., Hu, M., Zhong, L. J., Wiedensohler, A., Liu, S. C., Andreae, M. O., Wang, W., and Fan, S. J.: Regional Integrated Experiments on Air Quality over Pearl River Delta 2004 (PRIDE-PRD2004): Overview, Atmospheric Environment, 42, 6157-6173, 10.1016/j.atmosenv.2008.03.025, 2008.

Zhu, J., Wang, S., Wang, H., Jing, S., Lou, S., Saiz-Lopez, A., and Zhou, B.: Observationally constrained modeling of atmospheric oxidation capacity and photochemical reactivity in Shanghai, China, Atmospheric Chemistry and Physics, 20, 1217-1232, 10.5194/acp-20-1217-2020, 2020.